Phase-Change Kinetics of Bi–Fe–(N) Layer for High-Speed Write-Once Optical Recording

2011 Jpn. J. Appl. Phys. 50 042601

(http://iopscience.iop.org/1347-4065/50/4R/042601)

Japanese Journal of Applied Physics **50** (2011) 042601 **REGULAR PAPER**
DOI: 10.1143/JJAP.50.042601

Phase-Change Kinetics of Bi–Fe–(N) Layer for High-Speed Write-Once Optical Recording

Sung-Hsiu Huang, Yu-Jen Huang, Hung-Chuan Mai, and Tsung-Eong Hsieh*

Department of Materials Science and Engineering, National Chiao Tung University, 1001 Ta-Hsueh Rd., Hsinchu, Taiwan 30010, R.O.C.

Received October 20, 2010; accepted January 14, 2011; published online April 20, 2011

In this work, we present the phase-change kinetics of Bi–Fe–(N) layers for write-once optical recording. *In situ* reflectivity measurement indicated that the phase-change temperature (T_x) of the Bi–Fe–(N) layers is strongly related to the heating rate. The T_x's were about 170 °C at low heating rates and approached the melting point of the Bi phase (i.e., 271.4 °C) at high rate of heating provided by laser heating. For a 100-nm-thick Bi–Fe–(N) layer, Kissinger's analysis showed that the activation energy of phase transition (E_a) = 1.24 eV, while the analysis of isothermal phase transition in terms of the Johnson–Mehl–Avrami (JMA) theory showed that the average Avrami exponent (m) = 2.2 and the appropriate activation energy (ΔH) = 5.15 eV. With the aid of X-ray diffraction (XRD) analysis, a two-dimensional phase transition behavior in the Bi–Fe–(N) layers initiated by the melting of the Bi-rich phase was confirmed. For optical disk samples with optimized disk structure and write strategy, the signal properties far exceeding the write-once disk test specifications were achieved. Satisfactory signal properties indicated that the Bi–Fe–(N) system is a promising alternative for high-speed write-once recording in the Blu-ray era.

1. Introduction

Optical disks are the most important external data storage devices for multimedia and personal data management at present because of their large recording capacity, interchangeability, and portability.[1–3] According to the data recording principle, optical disks can be divided into read-only memory (ROM), write-once/recordable (R), and rewritable (RW). Among these, the write-once type is always the dominant product in the optical disk market and much effort has been exerted into studies of recording materials, either organic or inorganic,[4] for such a type of optical disk. At present, recording materials compatible with blue-laser recording are of particular interest. For such materials, organic ones are dyes that are sensitive to blue irradiation while inorganic ones include phase-change-based alloys,[5,6] AgInSbTe–SiO_2 nanocomposite films,[7,8] single layer metals such as AlSi alloys,[9,10] bismuth oxide (BiFeO)[11–13] and Bi–Fe–(N) layer,[14] and bilayer metals such as Ge/Au,[15–18] Cu/Si,[19] ZnO/Ge,[20] amorphous silicon (a-Si)/Cu,[21–24] a-Si/Al,[24,25] a-Si/Ni,[26–28] and Bi/Ge.[29,30]

In our previous study,[14] the Bi–Fe–(N) system was demonstrated to be a promising medium for high-density write-once recording. In contrast to the other recording media listed above, Bi–Fe–(N) exhibits a unique recording mechanism involving element separation and grain coarsening. Further study is thus required so as to gain a full understanding of its phase-change kinetics. In this work, an exothermal experiment in conjunction with Kissinger's analysis and an isothermal experiment in conjunction with Johnson–Mehl–Avrami (JMA) analysis are carried out. The correlations between optical property and microstructure changes of the Bi–Fe–(N) layer are presented so as to delineate its phase-change kinetics during laser irradiation. Write-once optical disk samples containing Bi–Fe–(N) recording layers were also prepared in accord with the high-density digital versatile disk (HD DVD) format, and their signal properties at 2× recording speed were evaluated in order to illustrate their feasibility for blue-laser optical recording.

2. Experimental Procedure

100-nm-thick Bi–Fe–(N) layers for phase-change kinetics study were deposited on Si substrates via sputtering deposition in a self-designed six-target sputtering chamber at a background pressure lower than 10^{-6} Torr. The thin-film samples were prepared by sputtering the Bi–Fe alloy target under Ar/N_2 gas flow at a working pressure of about 2 mTorr. A self-designed reflectivity-temperature measurement system was adopted to evaluate the *in situ* reflectivity change of the thin films as a function of temperature during the exothermal and isothermal experiments. The data obtained were then analyzed in accord with the Kissinger's theory and the JMA theory, respectively, so as to explore the phase-change behaviors of Bi–Fe–(N) layers. *In situ* heating X-ray diffraction (XRD) measurements were carried out at the beamline BL01C2 of the National Synchrotron Radiation Research Center (NSRRC) at Hsinchu, Taiwan, R.O.C., with an X-ray wavelength of 0.1033 nm, a 2θ angular range up to 60° and a fixed X-ray grazing incident angle at 1°. Such an XRD measurement collects the diffraction signals from a heated sample so as to explore the evolution of its crystal structure with a change in temperature. The samples were placed in a heating cell with argon (Ar) as the protecting gas, and the heating rate was maintained at 1 °C/min. A Mar 345 image plate detector was placed about 27 cm from the sample position and each image frame took 30 s for exposure during the measurements. The structural changes of the Bi–Fe–(N) layers were also characterized using an in-house X-ray diffractometer (MAC Science M18XHF) with Cu Kα radiation ($\lambda = 0.1542$ nm) at a scanning rate of 2°/min. The sample for in-house XRD measurement was first heated to various temperatures (170, 300, and 400 °C) for 30 min, cooled down to room temperature, and then placed in the XRD apparatus for characterization.

Since the accessible signal tester was previously built for HD DVD optical disks, we thus prepared disk samples containing the Bi–Fe–(N) recording layer in accord with the HD DVD specifications.[31,32] It is presumed that the results presented as follows may be equally applied in Blu-ray disks (BDs) since the emphasis of this study is on material characterizations, rather than on disk hardware. Figure 1 shows a cross-sectional view of optical disk sample deduced by structure and write strategy optimization. The signal properties of the disk samples including partial response signal-to-noise ratio (PRSNR), simulated bit error rate (SbER), modulation, and optimum write power (P_w), were evaluated using a dynamic tester (PULSTEC ODU-1000) equipped

*E-mail address: tehsieh@mail.nctu.edu.tw

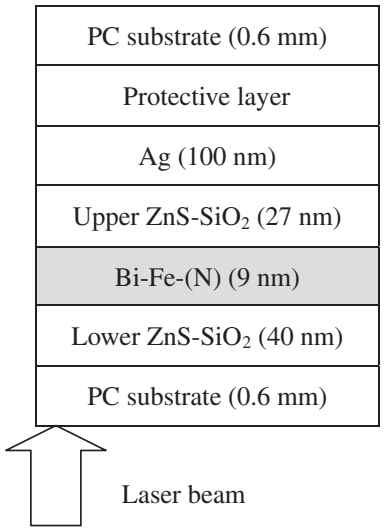

Fig. 1. Cross-sectional view of optical disk samples deduced by structure and write strategy optimization.

Table I. Conditions for dynamic test.[31,32]

	Recording speed	
	1×	2×
User capacity (Gbyte)	15	←
Thickness of substrate (mm)	0.6	←
Wavelength (nm)	405	←
Numerical aperture	0.65	←
Modulation code	ETM, RLL(1, 10)	←
Track pitch (μm)	0.4	←
Equalizer (dB)	6	←
Channel clock frequency (MHz)	64.8	129.6
Liner velocity (m/s)	6.61	13.22
User bit rate (Mbyte/s)	36.55	73.1

with a 405 nm laser diode and a numerical aperture (NA) of 0.65. The characterization was performed at a clock frequency = 64.8 to 139.6 MHz, a linear speed = 6.61 to 13.22 m/s, an equalizer = 6.0 dB, and a track pitch = 0.4 μm. Signal readout was carried out at a laser power (P_r) = 0.4 mW. The detailed conditions for dynamic test are listed in Table I.[31,32]

The microstructures as well as the composition changes of the optical disk samples subjected to laser writing were examined using a transmission electron microscopy (TEM; JEOL FX-II 2010) equipped with an energy dispersive spectrometer (EDS; Link ISIS 300). The plan-view TEM (PTEM) samples were prepared in terms of the method reported by Chen *et al.*[33] The disk sample was first cut into small pieces using scissors. After dissolving the PC substrate in CH_2Cl_2 solution, the specimen was mounted on a copper (Cu) mesh and transferred to the TEM for microstructure characterization.

3. Results and Discussion

3.1 Phase-change kinetics of Bi–Fe–(N) layers

Figure 2 shows the *in situ* reflectivity changes of the 100-nm-thick Bi–Fe–(N) layer heated at various rates of 2.5, 5, 7.5, and 10 °C/min. Accordingly, the phase-transition

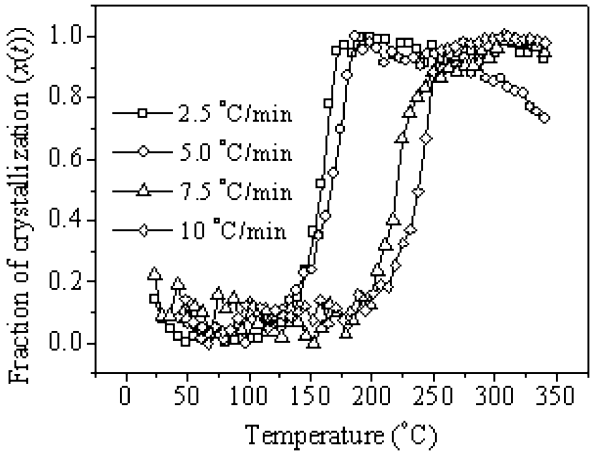

Fig. 2. Fraction of crystallization [$x(t)$] as function of temperature for Bi–Fe–(N) layer at various heating rates (film thickness = 100 nm).

Table II. T_x's for the Bi–Fe–(N) layers measured at various heating rates (film thickness = 100 nm).

Heating rate (°C/min)	T_x (°C)
2.5	165
5	175
7.5	217
10	243

temperatures (T_x's), i.e., the temperatures corresponding to the maximum reflectivity changes, could be determined by the derivation method, and the T_x's for various heating rates are listed in Table II. It can be seen that T_x increases with an increase in heating rate. This is ascribed to the superheat effects showing that the resistance to heat propagation in the samples increases with an increase in heating rate, causing a rise in T_x and thus a delay in phase transition. In particular, the T_x's indicate that phase transition in the Bi–Fe–(N) layer emerges at approximately 170 °C at low heating rates (e.g., below 5 °C/min) and, when the heating rate is high (e.g., above 5 °C/min), the phase change occurs at approximately 220 °C or above. As revealed by the XRD characterization and JMA analysis reported below, phase transition in the Bi–Fe–(N) layer is found to result from the melting of the Bi-rich phase. Although the T_x's listed in Table II are less than the melting point of pure Bi at 271.4 °C (= T_m^{Bi}), it is presumed that the T_x of Bi–Fe–(N) approaches T_m^{Bi} during signal writing owing to the extremely high heating rate of laser irradiation. In the present study, the deviation of T_x's from T_m^{Bi} is attributed to the liquidus behavior due to the formation Bi-rich alloy as well as to the presence of finely dispersed nitrides in the Bi–Fe–(N) layer[14] which may induce the melting transition in a heterogeneous manner. It is speculated that, once phase transition occurs, the molten Bi phase quickly becomes wet and forms an interpenetrating liquid network in the sample so as to induce a catastrophic phase transition. This explains why the phase transition of the Bi–Fe–(N) layer could be completed in a rather narrow temperature span (≤25 °C), as shown in Fig. 2 in comparison with other write-once recording media.[5–30] For instance, in the a-Si/Cu system, the precipitation of

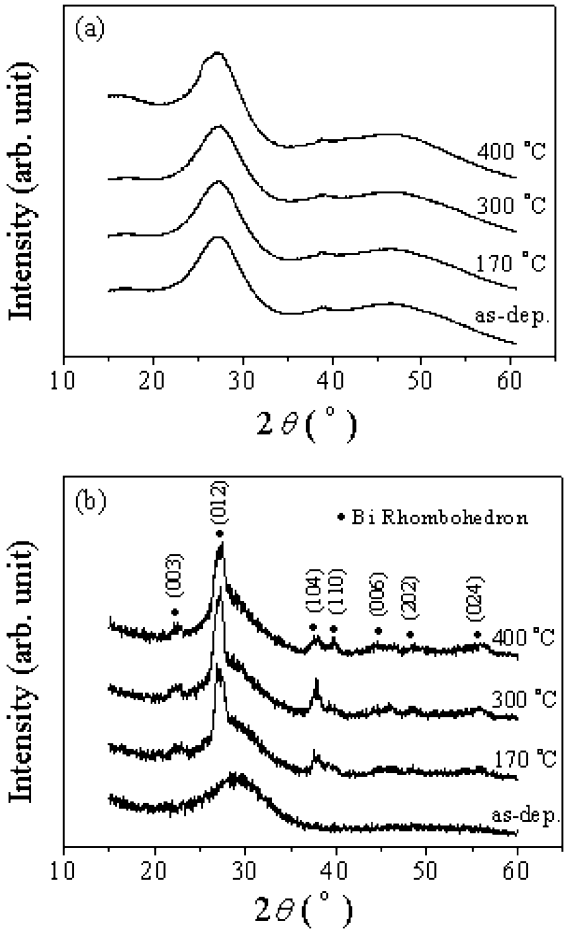

Fig. 3. XRD patterns of the samples acquired by (a) *in situ* heating XRD experiment and (b) in-house XRD analysis of the sample subjected to various heat treatments followed by cooling down to room temperature.

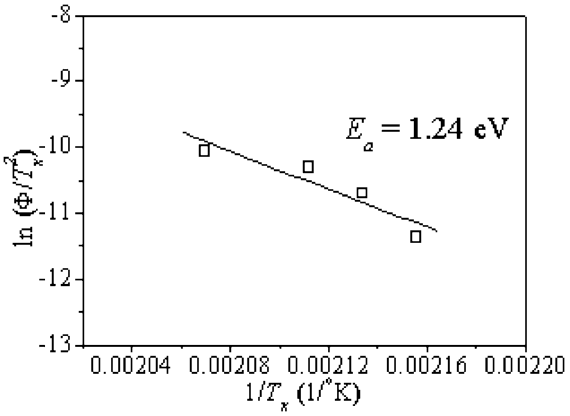

Fig. 4. Kissinger's plot for the Bi–Fe–(N) layer (film thickness = 100 nm).

the Cu_3Si phase followed by the recrystallization of amorphous Si occurs in a relatively wide temperature span ranging from 100 to 500 °C.[23,24] This also implies that the phase transition in the Bi–Fe–(N) layer proceeds in a relatively fast manner via the evolution of the molten Bi phase, which greatly benefits the high-speed signal writing when adopted as the recording media of optical disks.

In situ heating XRD analysis, i.e., acquisition of diffraction data during the isothermal heating of the samples, was employed to clarify the occurrence of the melting of the Bi-rich phase. A previous study showed that the as-deposited Bi–Fe–(N) layer is amorphous.[14] Since the molten phases remain amorphous, as shown in Fig. 3(a), only a fuzzy, broad peak emerges in the sample regardless of its heating temperature. This indicates that the melting of the Bi-rich phase in the Bi–Fe–(N) layer likely occurs during heating. The samples subjected to various heat treatments followed by cooling down to room temperature were also characterized by in-house XRD analysis. Figure 3(b) shows the characteristic peaks of the crystalline Bi phase (JCPDS file card No. 44-1246) that should form via the solidification of the molten Bi phase due to sample cooling. According to the results of XRD analysis presented above, the abrupt changes in the reflectivity profiles shown in Fig. 2 can thus be ascribed to Bi melting in the Bi–Fe–(N) layer.

The phase-change kinetics of the Bi–Fe–(N) layers were analyzed by utilizing Kissinger's equation[34] for the exothermal experiment and the JMA theory for the isothermal heating experiment, respectively. By plugging the data shown in Fig. 2 into Kissinger's equation,

$$\ln\left(\frac{\Phi}{T_x^2}\right) = C - \frac{E_a}{k_B T_x},$$

where Φ is the heating rate, E_a is the activation energy, k_B is the Boltzmann constant, and C is the constant, we obtained Kissinger's plot shown in Fig. 4. According to the slope of Kissinger's plot, E_a is about 1.24 eV.

For JMA analysis, the fraction of crystallization $[x(t)]$ was first calibrated from the results obtained by isothermal reflectivity measurements utilizing the relation

$$x(t) = \frac{R_t - R_0}{R_{max} - R_{min}},$$

where R_t and R_0 are the reflectivities measured at $t = t$ and $t = 0$, while R_{max} and R_{min} are the maximum and minimum reflectivities observed during the experiment, respectively. The extrapolation of $x(t)$ against t was then performed to determine the incubation period (τ_0) so that the data corresponding to the steady-state nucleation of phase transition could be extracted for subsequent analysis. Afterward, the Avrami exponent, m, and an appropriate activation energy, ΔH, were determined using the JMA equation[35–38]

$$x(t) = 1 - \exp[-\kappa(t - \tau_0)^m],$$

in which the coefficient κ can be expressed as

$$\kappa = \kappa_0\left(-\frac{\Delta H}{k_B T}\right).$$

We note that isothermal heating of Bi–Fe–(N) samples can only be carried out at temperatures below 170 °C since the onset of isothermal phase transition becomes unstable when the the sample is heated over 170 °C. This observation also supports a fast, catastrophic phase transition in the Bi–Fe–(N) layer induced by the melting of Bi-rich phase.

According to the plots of $\ln[-\ln(1-x)]$ against $\ln t$ shown in Fig. 5(a) and of $\ln\kappa$ against $1/T$ shown in Fig. 5(b), the averages of m and ΔH are 2.2 and 5.15 eV, respectively. The Avrami kinetic law predicts a two-

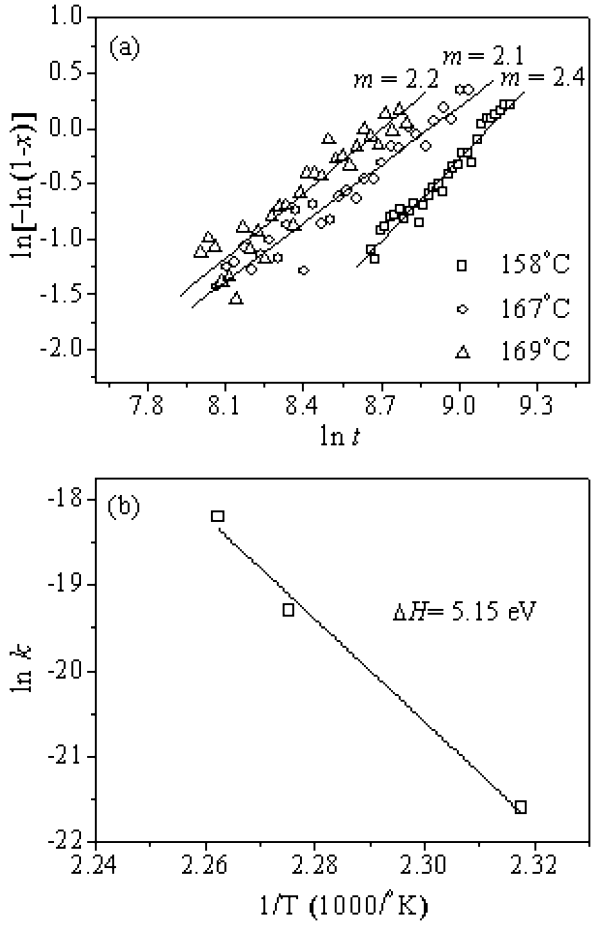

Fig. 5. Plots of (a) $\ln[-\ln(1-x)]$ against $\ln t$ and (b) $\ln \kappa$ against $1/T$ for the Bi–Fe–(N) layer (thicknesses = 100 nm).

dimensional phase transition behavior when $2 \leq m \leq 3$.[35–38] This is in good agreement with a previously proposed argument that the phase transition is induced by the wetting of a molten Bi-rich phase in the Bi–Fe–(N) layer since wetting is essentially a two-dimensional physical process.

Table III shows a summary of the T_x's and activation energies (E_a and/or ΔH) of phase transitions for various recording media reported previously.[6–8,15–18,20–30] Note that the T_x of the Bi–Fe–(N) system is listed at a temperature about 270 °C since an extremely high heating rate of laser irradiation leads to the similarity of the T_x of Bi–Fe–(N) system to T_m^{Bi}. As shown in Table III, the T_x of the Bi–Fe–(N) system is comparatively lower than those of bilayer media, but higher than those of phase-change materials. Furthermore, the low activation energy feature and the unique recording mechanism presented above indicate that the Bi–Fe–(N) system is a promising material for high-speed write-once recording in the Blu-ray era.

Finally, our JMA analysis shows that the ΔH for the Bi–Fe–(N) system seems to be high, as listed in Table III. According to JMA theory, ΔH is the sum of the activation energies of nucleation and growth processes. The high ΔH may have resulted from the dispersed solid nitrides and Fe-rich phase in the Bi–Fe–(N) layer that form the obstacles of grain growth. This increases the activation energy of the growth process and hence the ΔH. We, however, note that the determination of τ_0 markedly affects the calculated values of m and ΔH.[39] Since various data handling methods were employed by different research groups, the ΔH's listed here are for reference purpose only.

Table III. Comparison of T_x's and activation energies of various write-once recording media. E_a is obtained by Kissinger's analysis,[34] while m and ΔH are obtained by JMA analysis.[35–38]

Material	T_x (°C)	E_a (eV)	m	ΔH (eV)	Measurement	Ref.
$Sb_{70}Te_{30}$	136	2.08	3.5	1.97	Optical/DSC	6
AgInSbTe–SiO_2	198	—	2.8	3.03	Optical	7,8
Ge/Au	310	—	—	—	Optical	15–18
ZnO/Ge	385	—	—	—	DSC	20
a-Si/Cu	485	3.3 ± 0.1	1.8	—	Optical	21–24
a-Si/Al	357	3.3 ± 0.2	1.6	—	Optical	24,25
a-Si/Ni	350	2.19 ± 0.08	—	—	Optical	26–28
Bi/Ge	270	—	—	—	DSC	29,30
Bi–Fe–(N)	~270	1.24	2.2	5.15	Optical	—

3.2 Signal properties and microstructures of disk samples

Figure 6(a) shows the PRSNR and SbER as functions of P_w of the disk samples deduced by dynamic test at 1× and 2× recording speeds. Table IV shows a summary of the optimum signal properties achieved in this study. The maximum PRSNR = 26.7, minimum SbER = 7.4×10^{-8}, and modulation = 0.7 were achieved at the optimized P_w = 7.1 mW for 1× recording, and that the maximum PRSNR = 23.8, minimum SbER = 2.2×10^{-7}, and modulation = 0.7 were achieved at the optimized P_w = 9.1 mW for 2× recording. This illustrates a good sensitivity of the disk containing the Bi–Fe–(N) recording layer at low P_w values for various recording speeds. Furthermore, it can be readily seen that the test results exceed the HD DVD specifications, which require that PRSNR ≥ 15 and SbER ≤ 5×10^{-5} at $P_w \leq 10$ mW for 1× recording[31] and that $P_w \leq 13$ mW for 2× recording.[32]

The eye patterns corresponding to random signals ranging from 2T to 11T, read directly from an oscilloscope at 1× and 2× recording speeds, are shown in Fig. 6(b). Note that the length of short-T marks has been modified in order to obtain the optimum signal properties. This allows random signals to be written perfectly in the optical disks containing the Bi–Fe–(N) recording layer.

Figure 7 shows a bright-field PTEM image of signal marks in a disk sample recorded at 2× recording speed in which seashell-like signal marks with various recording lengths residing in the groove regions of disk sample can be clearly seen. In comparison with that reported in previous study,[14] the change in recording speed barely affects the morphology and sizes of grains in the signal marks. As shown in Fig. 7, the selected area electron diffraction (SAED) patterns taken from the nonmark and mark areas all exhibit vague ring patterns, indicating that the Bi–Fe–(N) layer remains amorphous before and after the signal writing. Apparently, signal writing in a Bi–Fe–(N) disk sample does not result in the recrystallization or formation of intermetallic phase in recording media as reported in other material systems.[15,24,40] Laser irradiation induces melting and element mixing in the Bi–Fe–(N) layer. When signal writing is completed, the rapid cooling preserves the

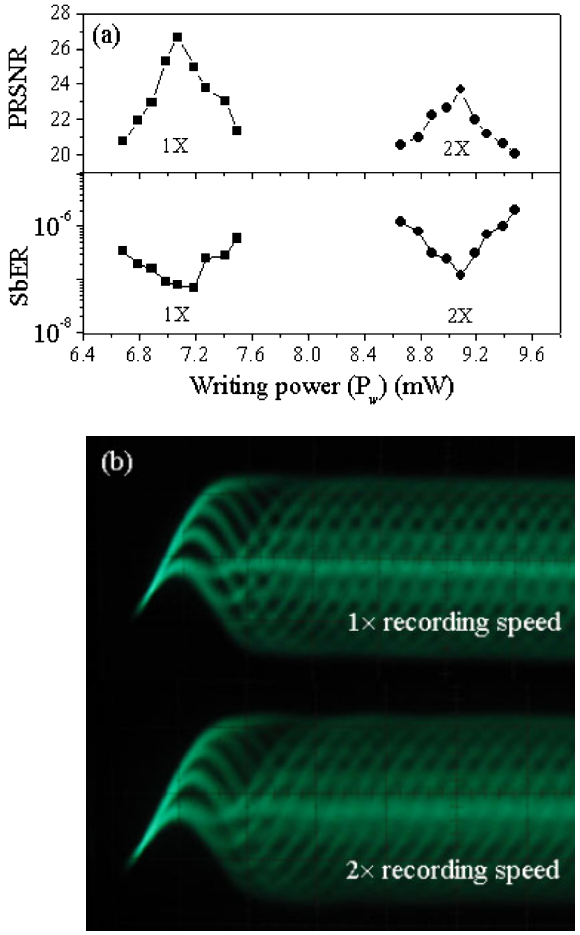

Fig. 6. (Color online) (a) Variations in PRSNR and SbER of disk samples as functions of P_w at various recording speeds and (b) the eye patterns of random signals read directly from the oscilloscope for the optical disk samples at 1× and 2× recording speeds.

Table IV. Optimum signal properties of Bi–Fe–(N) disk sample at various recording speeds.

	Recording speed	
	1×	2×
P_w (mW)	7.1	9.1
Record condition	Multi tracks	Multi tracks
PRSNR	26.7	23.8
SbER	7.4×10^{-8}	2.2×10^{-7}
Modulation	0.7	0.7

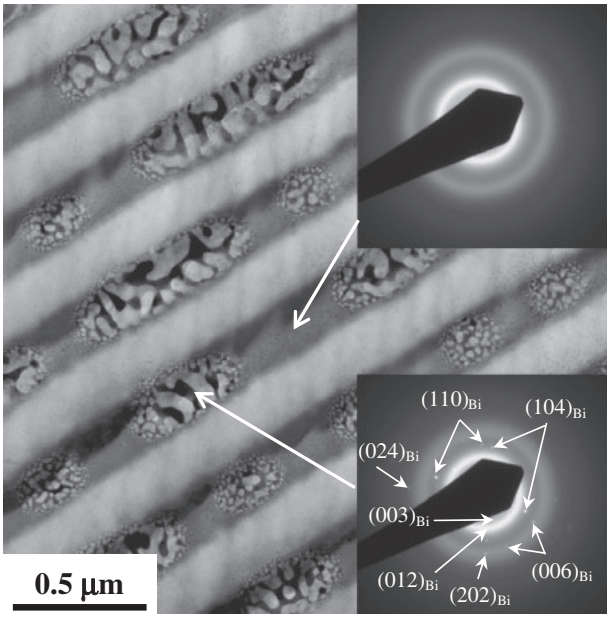

Fig. 7. Bright-field PTEM image of signal marks in the optical disk sample recorded at 2× recording speeds. The SAED patterns attached to upper- and lower-right-hand corners of the TEM image were taken from the nonmark and mark areas indicated by arrows, respectively.

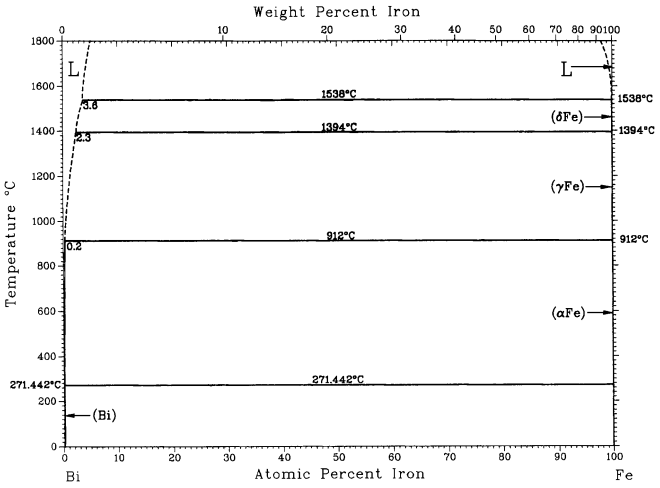

Fig. 8. Bi–Fe binary alloy phase diagram.[41]

amorphism of the molten phase, and the separation of Bi and Fe elements occurs simultaneously owing to the decrease in their mutual solubility with a decrease in temperature as indicated by the Bi–Fe binary alloy phase diagram[41] shown in Fig. 8. Element separation in the mark area[14] is elucidated in Fig. 9, which shows the EDS analytical result of the mark and its vicinity in a disk sample subjected to 2× recording. The recording mechanism of optical disks containing the Bi–Fe–(N) layer is hence attributed to the element separation accompanied by the coalescence/coarsening of separated phases, leading to sufficient change in optical properties for the signal readout of disk samples.

As shown in Fig. 7, there are bright diffraction spots in the SAED pattern taken from the mark area. TEM occasionally enabled the observation of these spots and, as indicated by the index of diffraction pattern in bottom right-hand corner of Fig. 7, the spots corresponds to the rhombohedral Bi phase. Some tiny Bi crystallites might form via heterogeneous nucleation during the solidification of a molten recording layer and the embedment of such fine Bi crystallites in the amorphous matrix of recording marks hence results in the SAED pattern shown in Fig. 7. Note that the index of the SAED pattern is in agreement with that of the in-house XRD profile shown in Fig. 3(b). Hence, the TEM analysis also supports the melting of the Bi-rich phase in the mark area proposed previously.

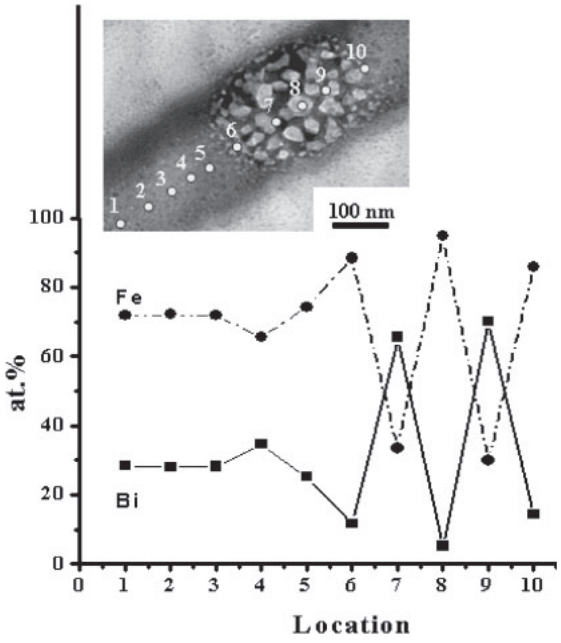

Fig. 9. Variations in chemical compositions deduced from the EDS analysis of the mark and its vicinity in a disk sample subjected to 2× speed recording. Locations of EDS analysis are indicated in the inset TEM image.

4. Conclusions

In this work, we present the analytical results of the phase-change kinetics of Bi–Fe–(N) layer for high-speed write-once optical recording. The exothermal experiment showed that the T_x of the Bi–Fe–(N) layer strongly depends on the heating rate that, at low heating rates, a phase change is induced at temperatures of about 170 °C. For practical laser heating, it would approach the melting point of Bi, i.e., 271.4 °C. Kissinger's analysis indicated that E_a is about 1.24 eV for a 100-nm-thick Bi–Fe–(N) layer. JMA analysis indicated that the average Avrami exponent is about 2.2 and the appropriate activation energy (ΔH) is 5.15 eV, revealing that the phase transition is accomplished by a two-dimensional wetting process due to the melting of the Bi-rich phase in the Bi–Fe–(N) layer. For the disk sample with optimized disk structure and write strategy, PRSNR = 26.7, SbER = 7.4×10^{-8}, and modulation = 0.7 were achieved at $P_w = 7.1$ mW for 1× recording and PRSNR = 23.8, SbER = 2.2×10^{-7}, and modulation = 0.7 were achieved at $P_w = 9.1$ mW for 2× recording. TEM/EDS characterizations confirmed that the recording mechanism of the Bi–Fe–(N) disk samples is correlated to the element separation in conjunction with grain coalescence/coarsening in the Bi- and Fe-rich phases. Satisfactory signal properties illustrate the promising applications of the Bi–Fe–(N) system to high-speed write-once recording in the Blu-ray era.

Acknowledgements

This work is supported by the National Science Council (NSC), Taiwan, R.O.C., under contract NSC96-2221-E-009-010. The dynamic test on optical disk samples supported by Prodisc Technology Inc., Taiwan, R.O.C., is deeply acknowledged. The authors would also like to thank for support in the XRD experiments, Dr. Chia-Hung Hsu, Dr. Hwo-Shuenn Sheu and Dr. Wei-Tsung Chuang of NSRRC, Hsinchu, Taiwan, R.O.C.

1) M. Takenaga, N. Yamada, K. Nishiuchi, N. Akahira, T. Ohta, S. Nakamura, and T. Yamashita: J. Appl. Phys. **54** (1983) 5376.
2) Y. Unno and K. Goto: Proc. SPIE **382** (1983) 32.
3) M. Terao, S. Horigome, K. Shigematsu, Y. Miyauchi, and M. Nakazawa: J. Appl. Phys. **62** (1987) 1029.
4) A. E. T. Kuiper and L. van Pieterson: MRS Bull. **31** (2006) 308.
5) N. Ishii, N. Kinoshita, N. Shimidzu, H. Tokumaru, H. Okuda, A. Hirotsune, Y. Anzai, M. Terao, and T. Maeda: Jpn. J. Appl. Phys. **41** (2002) 1691.
6) Y. S. Hsu, Y. D. Liu, Y. C. Her, S. T. Cheng, and S. Y. Tsai: Jpn. J. Appl. Phys. **47** (2008) 6016.
7) H. C. Mai and T. E. Hsieh: Jpn. J. Appl. Phys. **46** (2007) 5834.
8) H. C. Mai, T. E. Hsieh, S. H. Huang, S. S. Lin, and T. S. Lee: Jpn. J. Appl. Phys. **47** (2008) 6029.
9) B. M. Chen and R. L. Yeh: Proc. SPIE **5380** (2004) 141.
10) B. M. Chen, H. F. Chen, R. L. Yeh, and J. M. Chung: Jpn. J. Appl. Phys. **43** (2004) 5018.
11) N. Sasa, Y. Hayashi, T. Fujii, K. Otaka, A. Watada, H. Kamezaki, and H. Komoda: Jpn. J. Appl. Phys. **43** (2004) 4972.
12) N. Sasa, Y. Hayashi, T. Fujii, A. Watada, and H. Komoda: Jpn. J. Appl. Phys. **44** (2005) 3643.
13) Z. Jiang, Y. Y. Geng, and D. H. Gu: Chin. Phys. Lett. **25** (2008) 3288.
14) H. C. Mai, T. E. Hsieh, S. Y. Jeng, C. M. Chen, and J. L. Wang: Appl. Phys. Lett. **92** (2008) 021906.
15) T. H. Wu, P. C. Kuo, Y. H. Fang, J. P. Chen, P. F. Yen, T. R. Jeng, C. Y. Wu, and D. R. Huang: Appl. Phys. Lett. **90** (2007) 151111.
16) T. H. Wu, P. C. Kuo, S. L. Ou, J. P. Chen, P. F. Yen, T. R. Jeng, C. Y. Wu, and D. R. Huang: Appl. Phys. Lett. **92** (2008) 011126.
17) Z. Chen, S. Zhang, S. Tan, J. Hou, Y. Zhang, and H. Sekine: J. Appl. Phys. **89** (2001) 783.
18) Z. Chen, S. Tan, S. Zhang, J. Hou, Z. Wu, and H. Sekine: Jpn. J. Appl. Phys. **40** (2001) 3960.
19) A. E. T. Kuiper, R. J. M. Vullers, D. Pasquariello, and E. P. Naburgh: Appl. Phys. Lett. **86** (2005) 221921.
20) C. P. Liu, Y. T. Hung, J. S. Tsai, G. J. Huang, and T. R. Jeng: Jpn. J. Appl. Phys. **46** (2007) 7365.
21) J. B. Lee, C. J. Lee, and D. K. Choi: Jpn. J. Appl. Phys. **40** (2001) 6177.
22) S. W. Russel, J. Li, and J. W. Mayer: J. Appl. Phys. **70** (1991) 5153.
23) Y. C. Her and C. L. Wu: Jpn. J. Appl. Phys. **43** (2004) 1013.
24) Y. C. Her, C. W. Chen, and C. L. Wu: J. Appl. Phys. **99** (2006) 113512.
25) Y. C. Her and C. W. Chen: J. Appl. Phys. **101** (2007) 043518.
26) Y. Kawazu, H. Kudo, S. Onari, and T. Arai: Jpn. J. Appl. Phys. **29** (1990) 729.
27) F. A. Ferri and A. R. Zanatta: J. Appl. Phys. **100** (2006) 094311.
28) Y. C. Her, S. T. Jean, and J. L. Wu: J. Appl. Phys. **102** (2007) 093503.
29) Y. Hosoda, T. Izumi, A. Mitsumori, F. Yokogawa, S. Jinno, and H. Kudo: Jpn. J. Appl. Phys. **42** (2003) 1040.
30) Y. Hosoda, A. Mitsumori, M. Sato, and M. Yamaguchi: Jpn. J. Appl. Phys. **43** (2004) 4997.
31) DVD Specifications for High-Density Recordable Disc (HD DVD-R) for blue laser optical system, Version 0.9, The DVD Forum (July 2004).
32) DVD Specifications for High-Density Recordable Disc (HD DVD-R) for blue laser optical system, Version 2.0, The DVD Forum (February 2007).
33) H. W. Chen, T. E. Hsieh, J. R. Liu, and H. P. D. Shieh: Jpn. J. Appl. Phys. **38** (1999) 1691.
34) H. E. Kissinger: Anal. Chem. **29** (1957) 1702.
35) M. Avrami: J. Chem. Phys. **7** (1939) 1103.
36) M. Avrami: J. Chem. Phys. **8** (1940) 212.
37) M. Avrami: J. Chem. Phys. **9** (1941) 177.
38) J. W. Christian: *The Theory of Transformations in Metals and Alloys* (Pergamon Press, Oxford, U.K., 1975) 2nd ed., Part I, p. 542.
39) V. Weidenhof, I. Friedrich, S. Ziegler, and M. Wuttig: J. Appl. Phys. **89** (2001) 3168.
40) Y. C. Her, J. H. Chen, M. H. Tsai, and W. T. Tu: J. Appl. Phys. **106** (2009) 023530.
41) T. B. Massalski: *Binary Alloy Phase Diagrams* (ASM International, Materials Park, OH, 1990) 2nd ed., p. 737.